



OPEN

SUBJECT AREAS:

ELECTRICAL AND
ELECTRONIC
ENGINEERING

NANOCAVITIES

Decorative power generating panels
creating angle insensitive transmissive
colors

Jae Yong Lee*, Kyu-Tae Lee*, Sungyong Seo & L. Jay Guo

Department of Electrical Engineering and Computer Science, The University of Michigan, Ann Arbor, Michigan 48109, USA.

Received
14 January 2014Accepted
30 January 2014Published
28 February 2014Correspondence and
requests for materials
should be addressed to
L.J.G. (lguo@umich.
edu)* These authors
contributed equally to
this work.

We present ultra-thin (6 to 31 nm) undoped amorphous silicon/organic hybrid solar cell structure, which can transmit desired color of light. The transmitted colors show great angular tolerance due to the negligible optical phase associated with light propagating in ultra-thin amorphous silicon (a-Si) layers. We achieved the power conversion efficiency of the hybrid cells up to 2 %; and demonstrated that most of the absorbed photons in the undoped a-Si layer contributed to the extracted electric charges due to the suppressed electron-hole recombination in the ultra-thin a-Si layer. We also show the resonance is invariant with respect to the angle of incidence up to $\pm 70^\circ$ regardless of the polarization of the incident light. Our exploration provides a design to realize energy harvesting colored photovoltaic panels for innovative applications.

Recently there have been increased interests in transparent photovoltaics (PV) for building integrated PV applications. Dye sensitized solar cells (DSSC) have been good candidates for transmissive colored solar cells by applying a variety of dyes¹. However, colors heavily depend on the types of dyes and their limited combinations. Moreover, dyes induce the transmitted light to be scattered and dimmed, making behind images blurry. Organic PV (OPV) has also been investigated for their feasibility in colored PV cells by combining various photoactive materials and electron acceptors². Due to flat and broad absorption capability of the materials, color tunability was limited in red or yellow, not available in blue or green.

Since color filters have been used in numerous areas, such as display technology as well as light emitting products, their integration with various PV panels can be considered. Recently a scheme was developed by integrating Fabry-Perot (F-P) cavities directly above OPV where the transmission colors with high color purity are created by the F-P filters³. However the F-P resonance wavelength will vary with incident angle and the polarization of the incident light, which will affect the color appearance of the solar cell. Many nanostructure based plasmonic and photonic color filters investigated in the past have also faced challenges in the resonance shift when light is incident upon the device at different angles^{4–7}. This resonance shift results in an undesirable color change. Therefore, there is a critical need to develop an incident angle robust color generating design that can be integrated with the PVs.

As the building integrated PVs typically target large areas, the materials of choice should be those that can be deposited or processed in large areas. OPV can satisfy this requirement, however they require barrier coating or hermetic sealing to prevent oxygen and moisture from affecting the device's performance⁸. There is another low-cost PV platform that can be easily scalable to large area, which is amorphous silicon based PVs⁹. Amorphous silicon (a-Si) has been used routinely in flat panel display industry and can be deposited by chemical vapor deposition over ~ 50 inch size glass panel. But traditional solar panels all look black due to the use of very thick semiconductor layers for maximum light absorption. Photon management for tuning transparency and color generation are not possible in traditional thick semiconductor PVs. In order to produce desired colors, especially for semi-transparent colored panels, the a-Si semiconductor layer should be only the order of 10–20 nm. Clearly the widely used p-i-n structure in traditional a-Si PVs cannot address this requirement because the doped layers alone already add up to 40–50 nm¹⁰.

We propose a hybrid PV structure by using metal oxide and organic interfacial charge transport layers with undoped a-Si. This allows us to use a very thin a-Si layer, which not only satisfies the requirement for semi-transparent color generation, but also offers several unique advantages. First, since the a-Si layer thickness is an order of magnitude thinner than the traditional a-Si PVs¹¹, the photo-carrier recombination is effectively minimized which leads to high quantum efficiency of the device. Second, distinct colors can be generated by resonant



optical transmission. But different from the F-P resonance where the net of round-trip propagation phase inside the cavity and the reflection phase is multiples of 2π , our structure utilized the extraordinary phase change of light reflecting from a light-absorbing medium (in this case a-Si) and metal interface to achieve the constructive light interference¹². A direct benefit of this is that we can achieve angle-insensitive colors due to the negligible phase change of light propagating through the ultra-thin a-Si layer as compared with the unusual reflection phase. Moreover, our structures are also insensitive to the polarization of the incident light, making it suitable for the semi-transparent decorative PV applications.

Results

The ultra-thin a-Si/organic hybrid solar cells are built on fused silica substrates, comprising an anode, an ultra-thin a-Si layer, and a cathode (Fig. 1a). The anode structure is designed to transmit a wide range of wavelengths. The electrodes are derived from the dielectric-metal-dielectric (DMD) structures that have been developed as ITO-free transparent electrodes^{13,14}. For the anode, the metal and dielectrics are silver (Ag), tungsten trioxide (WO_3) and vanadium pentoxide (V_2O_5). In particular V_2O_5 is interfaced with a-Si and utilized as a transporting layer for the photogenerated holes due to its high work function¹⁵. A thin Ag (11 nm) is sandwiched between the two dielectric layers in the anode; here the Ag thickness determines the conductivity of the electrode, of which a sheet resistance below 10 ohm/\square is obtained. Perylenetetracarboxylic bis-benzimidazole (PTCBI)¹⁶ is used as a wetting layer underneath the Ag in order to form a smooth and continuous Ag thin film. We did not use Ge as the wetting layer for Ag due to its strong absorption in the visible range¹⁷.

The cathode begins with a thin organic layer, indene- C_{60} bisadduct (ICBA)¹⁸, which operates as a very efficient photogenerated

electron transport layer since its lowest unoccupied molecular orbital (LUMO) level is well aligned with a-Si conduction energy band. The ICBA is followed by another organic material of bis-adduct fullerene surfactant (C_{60} surfactant)¹⁹, which effectively lowers the Ag work function and forms ohmic contact for the electrons. The cathode is completed with the combination of Ag and WO_3 with different thicknesses according to our theoretical calculation (Fig. 1a). All the anode and cathode materials, except ICBA and C_{60} surfactant, were thermally evaporated consecutively without breaking the vacuum (base pressure 1×10^{-6} mbar). The ICBA and C_{60} surfactant were spin casted all in the same conditions as well. The undoped a-Si layers were deposited by using a plasma enhanced chemical vapor deposition (PECVD) tool. To produce the blue, green and red colors, 6, 11, and 31 nm of a-Si were deposited, respectively.

In our anode design, a thin Ag layer is also utilized to increase the reflection at the interface with V_2O_5 , consequently enhancing a quality factor (Q-factor), which yields a narrow resonance bandwidth. Ag is selected for both top and bottom electrode since Ag has the highest reflectivity and the lowest absorption at visible frequencies. A strong resonance behavior arises from the cavity comprising a highly lossy material, a-Si, sandwiched by the two electrodes. Though ICBA, C_{60} surfactant, and V_2O_5 layers can contribute to the resonance, we found that the resonance is primarily determined by the a-Si layer due to the high refractive index of a-Si. The detailed information about the resonance can be found in Supplementary Information.

The calculated (solid line) and the measured (dotted line) transmission spectra of individual colors of devices with varied a-Si thickness at the normal incidence are depicted in Fig. 1b. We performed all the optical simulation by using a transfer matrix method based on the measured refractive index of each material. The experimental spectra show an excellent agreement with the simulated profiles.

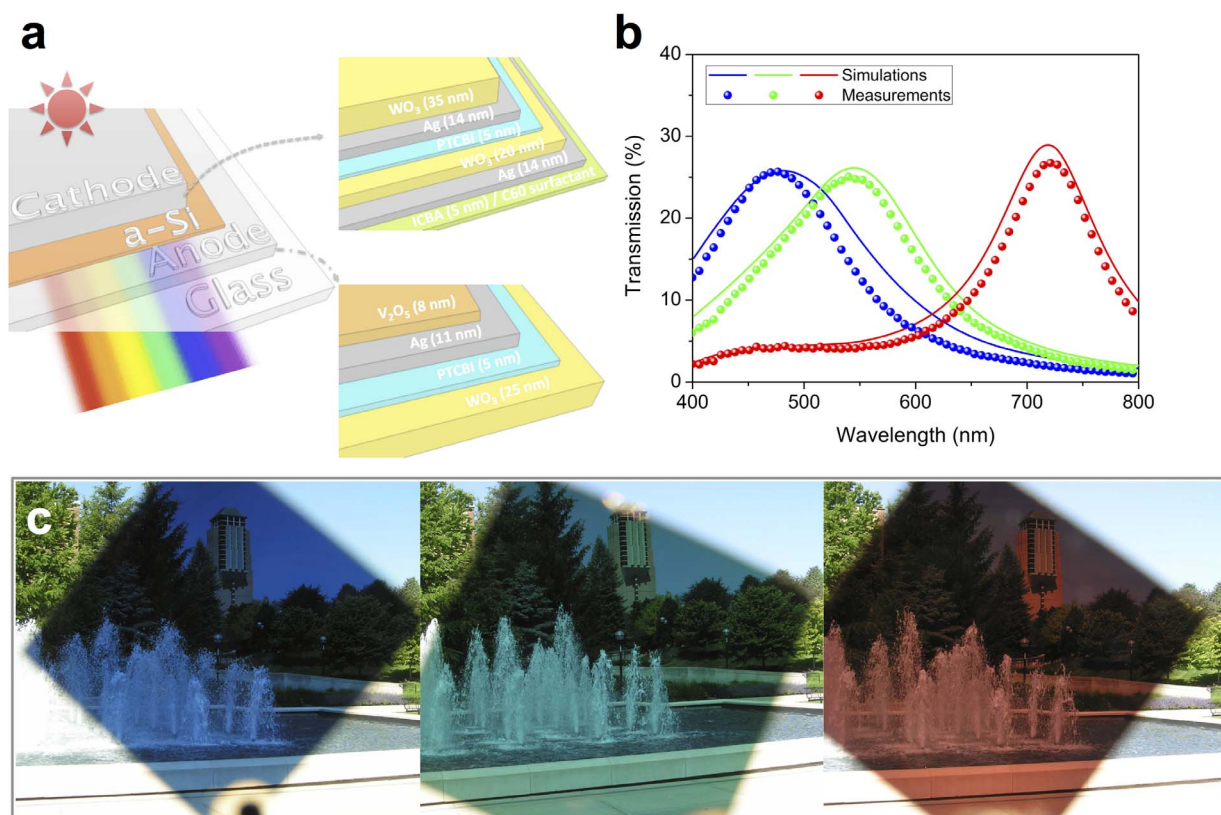


Figure 1 | Device structure and optical property. (a) A schematic diagram of proposed structure. The structure comprises cathode, anode, and ultra-thin undoped a-Si. The cathode is composed of dielectric-metal-dielectric (DMD) and organic layers, and only DMD structure for the anode. The ultra-thin a-Si layer thickness is 6, 11, and 31 nm for blue, green, and red, respectively. (b) Calculated and measured transmission spectra of individual colors (blue, green, and red) at normal incidence. (c) Photographs of distinct blue, green, and red colors by the fabricated devices.



The a-Si thicknesses of 6 nm, 11 nm, and 31 nm determine the transmission peaks located at 478 nm (blue), 542 nm (green), and 720 nm (red), respectively, while the thicknesses of all other layers remain the same for all devices. This simple fabrication process involving only film deposition can be easily scaled to large area substrate for industry level production.

The photograph images of fabricated samples are shown in Fig. 1c. It is obvious to see the water fountain and buildings through our devices with distinct colors. It is noteworthy to mention that there is no change in color even with oblique angles of incidence, which will be discussed more in detail in the following section.

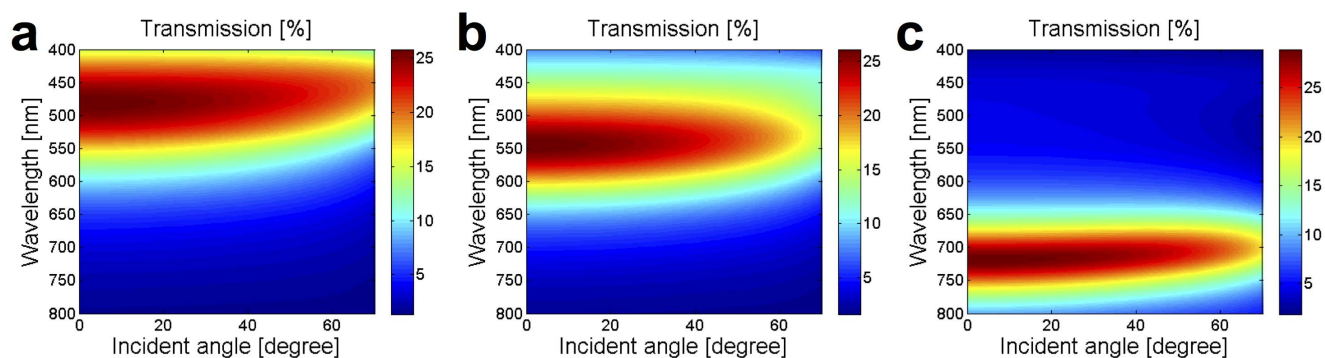
To investigate the angular dependence of our decorative panels, we performed a simulation: the calculated dispersion curves are illustrated in Fig. 2a–c. The flat dispersion curves indicate that the resonance wavelengths of the blue, green, and red colored devices are retained up to $\pm 70^\circ$. This angle insensitivity is experimentally verified by the measured transmittance of the devices for incident angle varying from 0 to 70° under unpolarized light illumination (Fig. 2d–f), which showed excellent agreement with the calculated profiles. As noted earlier the resonant wavelength in conventional F-P cavity is inherently related to the angle of incidence. The angle robustness of our devices is due to the use of ultra-thin a-Si, which results in relatively insignificant phase change accumulated as light propagates through the a-Si layer as compared to the phase shift upon reflection at the interface. Thus the resonance can remain fairly unvaried as the angle of incidence increases. The angle robustness and wide angle acceptance are also beneficial for the solar panel deployment in which no external sun tracking systems are needed. Another important feature of our device is the polarization independence. As all

common light sources, including the sun, fluorescent, and ambient light, produce unpolarized light, our proposed devices can utilize all sources of light to generate electricity efficiently. The angular dependences for transverse electric (TE) and transverse magnetic (TM) polarization were explored as well and can be found in Supplementary Information.

For the blue, green, and red device types (Fig. 3a), absorption spectra of a-Si active layers versus wavelength were calculated as shown in Fig. 3b. Remarkably, the electrically measured external quantum efficiency (EQE) profiles are well matched with the calculated absorption spectra. The EQE spectrum represents actual incident photon-to-charge conversion efficiency and is determined by the light absorption in the active layer and the internal quantum efficiency of the photoactive/transporting layers. The close match between the calculated a-Si absorption and the measured EQE curves implies that the internal quantum efficiency is approaching 100 %. This can be attributed to the strongly suppressed electron-hole recombination in our ultra-thin a-Si hybrid cells.

Regardless of device types (blue, green, or red), the a-Si layer thickness is much thinner than the typical charge diffusion length in a-Si^{20,21} so most photogenerated charges are extracted to the metal contacts through the electron and hole transporting layers. Furthermore the suppressed charge recombination can significantly mitigate the light-induced degradation, which is a drawback of traditional a-Si solar cells^{22–24}. Many previous studies have focused on optimizing p- and n- layer thicknesses to lessen the charge loss in the doped regions without sacrificing an internal electric field²⁵. Our devices with undoped a-Si active layer do not suffer from the charge recombination with p- and n- dopants as in the traditional a-Si PV,

Simulation



Measurement

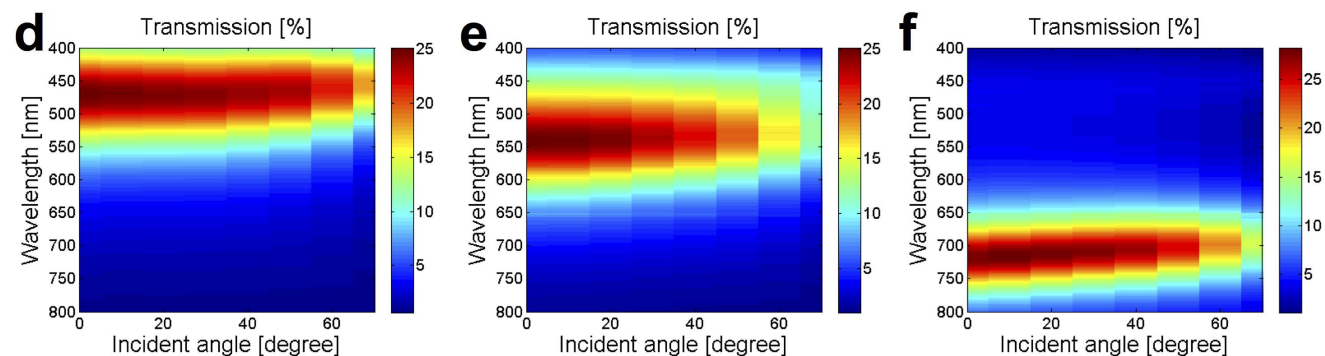


Figure 2 | Simulated and measured angular dependence under unpolarized light illumination. (a)–(c) Calculated angular behaviors of blue (6 nm), green (11 nm), and red (31 nm) devices, respectively, show that the resonance corresponding to the peak (red in the color map) in the transmission spectra remains at fairly same level over a relatively wide range of incidence angle up to 70° . The color bars denote how much the light is transmitted through the whole device. (d)–(f) Measured incidence angle dependence corresponding to those in (a)–(c).

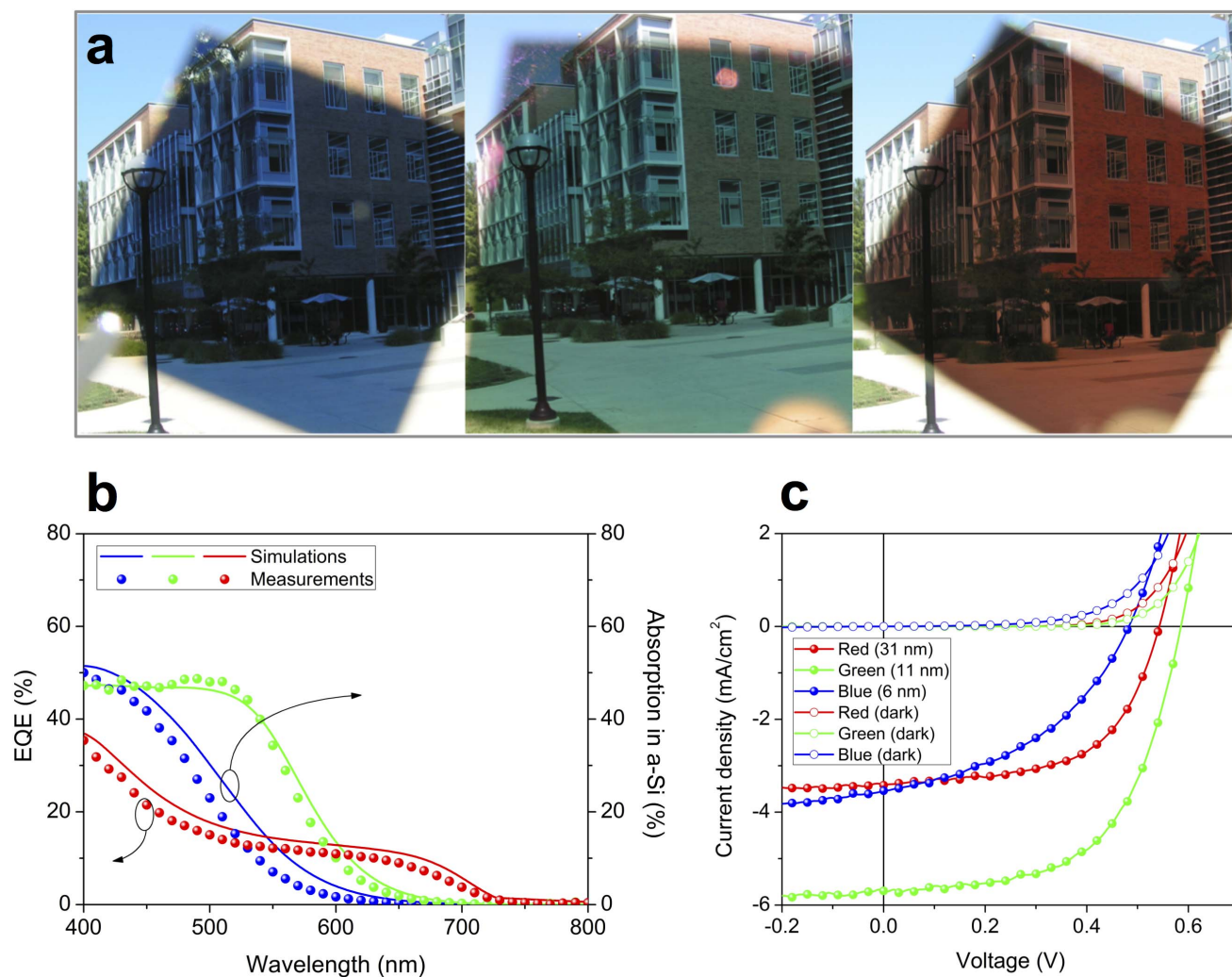


Figure 3 | Numerical simulation for a-Si absorption and electrical performance of the hybrid cells. (a) The pictures of the devices transmitting blue, green, and red colors. (b) Comparison of calculated incident light absorption profiles by ultra-thin a-Si layer and measured external quantum efficiency (EQE) spectra for three different types of devices (blue, green, and red). (c) Current density-voltage characteristics of the hybrid cells under AM1.5 illumination and dark conditions.

which is one of the major charge loss mechanisms in p-i-n a-Si solar cells^{25–27}.

Because the EQE of our devices directly correlates with the calculated light absorption in a-Si layer, we can estimate the electric current from the simulated optical absorption spectrum in an active layer with good accuracy. As the total number of photons absorbed in the active layer is very similar to the total extracted charges, we can design the electric current performance of the solar cells simply based on the optical calculation before fabricating devices. Based on this understanding, an interesting finding is that we expect to obtain higher photocurrent from the green color cell than the red cell (Fig. 3b), even though the a-Si layer thickness for the former (11 nm) is much thinner than that of the latter (31 nm).

To verify this prediction, we measured current density-voltage characteristics under AM1.5 illumination and dark conditions. The device measured has a diameter of 1 mm as in EQE characterization. The current density-voltage curves in Fig. 3c show the average efficiency performance of multiple devices for each type (red, green, or blue). As we expected from the calculated light absorption in the a-Si layer and EQE spectra previously, the green device has much higher current density (5.69 mA/cm²) than the red one (3.42 mA/cm²) with comparable fill factor (58~59 %). The green color device generates almost 2 % power efficiency by only 11 nm of a-Si active layer. This is

a remarkable result if comparing with the ~10 % efficiency obtained in traditional a-Si PV with more than twenty folds a-Si thickness²⁸. More detail power conversion efficiency factors of the three types of devices are summarized as a table in Supplementary Information.

Most prominently, the blue color device with only 6 nm of a-Si active layer operated well as a solar cell even though the fill factor of the blue device is lower than the other types of devices. We presume that a few nanometer a-Si active layer of the blue device induces more electric charge leaking paths in the device area, thereby reducing shunt resistance of the solar cell compared to the red and green devices that have thicker a-Si active layers.

Experimentally, we have confirmed that three types of devices (red, green, and blue) worked well for electric power conversion, generating short circuit current density as designed in our optical simulation. Other thin-film inorganic materials can potentially borrow this novel concept of our hybrid cells for higher power efficiency, filtering various colors based on appropriate photon management in their active layers.

As a further demonstration, we fabricated a 3 in × 2.3 in power-generating sample in the form of the national flag of the United States (U.S. flag) shown in Fig. 4a. The blue and red regions of the flag use a-Si thickness of 6 nm and 31 nm, respectively, same as in the individual colored samples discussed earlier. In addition, an angle of

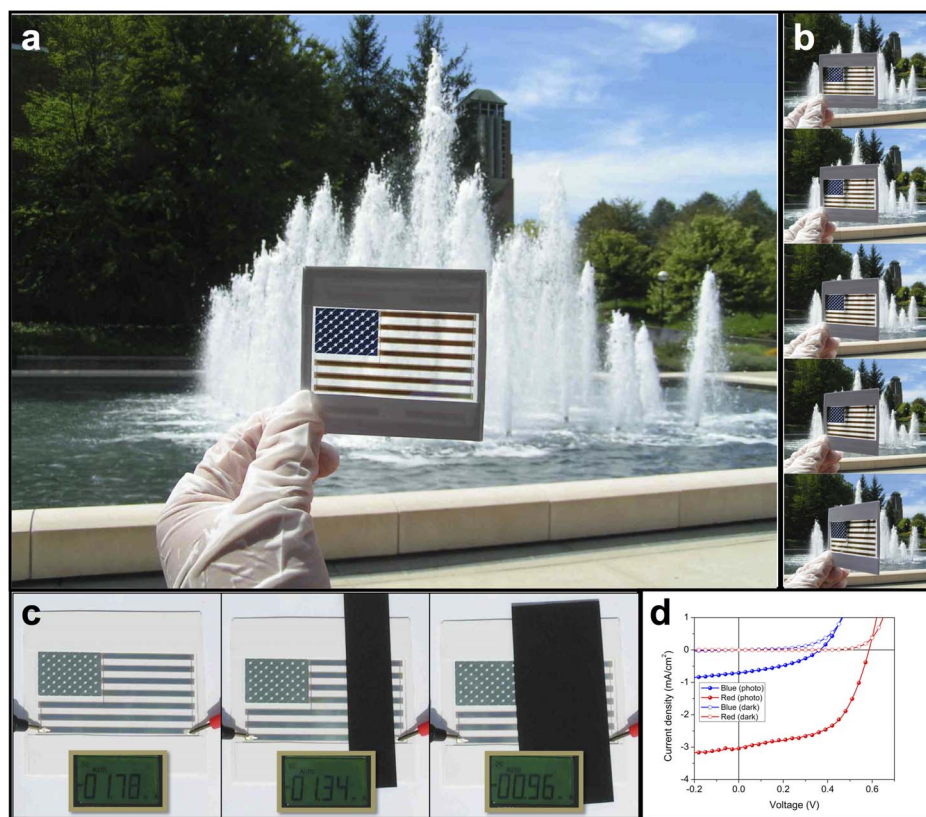


Figure 4 | The demonstration of the electric power-generating national flag of the United States of America (U.S. flag). (a) Photograph of the U.S. flag taken at the University of Michigan campus shows distinct blue (6 nm) and red (31 nm) color patterns. (b) According to angle insensitive property, the U.S. flag maintains its colors at oblique angles of incidence up to about 60°, manually controlled. (c) The U.S. flag generates electric current as well under outdoor sunlight (less than AM1.5). The electric current level decreases as the U.S. flag gets covered more by a piece of black paper. (d) Current density-voltage performances of blue and red colored 1 mm diameter devices under AM1.5 illumination.

incidence is changed from normal to 60° in order to verify the angle invariance performance of the power-generating U.S. flag. Indeed, the distinct blue background of the stars and the red stripes in the U.S. flag can maintain their respective colors at oblique angles of incidence as described in Fig. 4b.

In terms of electric power performance, the total colored regions (~1.5 in²) of the U.S. flag generates almost 2 mA electric current under real outdoor sunlight (less than AM1.5) with full light exposure to the flag (Fig. 4c). When the flag is partially covered by a piece of black paper, the current level evidently drops by the ratio of the unblocked flag area. We also measured current density-voltage characteristics by 1 mm diameter devices in the same U.S. flag sample (Fig. 4d). We note that the other transmission colors can be readily realized by simply tuning the a-Si layer thickness.

Discussion

We have demonstrated that a-Si/organic hybrid cells with varied undoped a-Si layer thickness can pass blue, green, and red colors. Simultaneous power generation is achieved with efficiency approaching 2 %. The use of ultra-thin a-Si layer leads to high angular tolerance of the transmitted colors. Notably, most of the absorbed photons in the undoped a-Si layer were converted to the electric charges benefited by the suppressed electron-hole recombination in the ultra-thin a-Si layer. We believe that this new principle can be easily employed in different inorganic materials systems as well so that the power-generating decorative panels can be applied to modern buildings. Potentially our colored panels can be utilized for other spectral selective applications including dual-function glass roof for the greenhouses to absorb green and ultraviolet light for electric

power generation while passing blue and red light to be absorbed by the chlorophyll for green plants' growth.

Methods

Optical and electrical characterizations. The optical simulation is carried out by using an optical transfer matrix method based on the refractive indices of all the materials measured by a spectroscopic ellipsometer (M-2000DI Ellipsometer, Woollam). For optical performance measurement, transmission spectra of the proposed decorative power generating cells for the incident angles from 0° to 70° were measured by using a spectrometer (HR4000CF, Ocean Optics) under unpolarized, TE-, and TM-polarized light illumination. The electrical property of the proposed decorative PVs was experimentally measured by current density-voltage (J-V) characterizations. The 1 mm diameter size circular-shaped devices were characterized under illumination by AM1.5 simulated sunlight (100 mWcm⁻²). We designed an optical setup to uniformly distribute the intensity of the light illumination throughout the cell area. For the data acquisition of electrical current and voltage in J-V measurements, Keithley 2400 is connected to the cathode and anode of solar cell devices. Power conversion efficiency of each decorative cell (red, green, or blue) was calculated by the average values of J_{sc} , V_{oc} , and FF obtained from multiple cells on the same substrate.

Device fabrication. First, we start with a fabrication of an anode comprising WO₃/Ag deposited by a thermal evaporation on a glass substrate, which shows a sheet resistance below 10 ohm/□. For a hole transporting layer, V₂O₅ was deposited at a rate of 0.2 Ås⁻¹ in the same chamber with a high vacuum (10⁻⁶ mbar). After that, an intrinsic a-Si layer was deposited by using a PECVD at 240°C (SiH₄ gas with 13.56 MHz RF power). As an electron transporting layer, the solution of ICBA with chlorobenzene solvent was spin-casted on the photoactive layer. The prior layers were covered by a transparent cathode consisting of WO₃/Ag that was deposited by using a thermal evaporation. In order to demonstrate the custom-made color and pattern of our a-Si hybrid cells, four steel shadow masks were designed for the U.S. flag, which generates an electric current under outdoor sunlight as exhibited in Fig. 4. The anode and cathode shadow masks were utilized in the thermal evaporator for the metal oxides or Ag depositions. In PECVD chamber, the blue and red pattern masks were applied to deposit the two different thicknesses of a-Si for blue and red colors in the U.S. flag, respectively.



1. Ahmad, S., Guillen, E., Kavan, L., Gratzel, M. & Nazeeruddin, M. K. Metal free sensitizer and catalyst for dye sensitized solar cells. *Energy Environ. Sci.* **6**, 3439–3466 (2013).
2. Ameri, T. *et al.* Fabrication, optical modeling, and color characterization of semitransparent bulk-heterojunction organic solar cells in an inverted structure. *Adv. Funct. Mater.* **20**, 1592–1598 (2010).
3. Chen Y.-H. *et al.* Microcavity-embedded, colour-tuneable, transparent organic solar cells. *Adv. Mater.* **26**, 1129–1134 (2014).
4. Xu, T., Wu, Y.-K., Luo, X. & Guo, L. J. Plasmonic nanoresonators for high-resolution colour filtering and spectral imaging. *Nat. Commun.* **1**, 59 (2010).
5. Yoon, Y.-T. *et al.* Color filter incorporating a subwavelength patterned grating in poly silicon. *Opt. Express* **16**, 2374–2380 (2008).
6. Diest, K., Dionne, J. A., Spain, M. & Atwater, H. A. Tunable Color Filters Based on Metal-Insulator-Metal resonators. *Nano Lett.* **9**, 2579–2583 (2009).
7. Kaplan, A. F., Xu, T. & Guo, L. J. High efficiency resonance-based spectrum filters with tunable transmission bandwidth fabricated using nanoimprint lithography. *Appl. Phys. Lett.* **99**, 143111 (2011).
8. Dennler, G. *et al.* A new encapsulation solution for flexible organic solar cells. *Thin Solid Films* **511–512**, 349–353 (2006).
9. Shah, A., Torres, P., Tscharnner, R., Wyrsh, N. & Keppner, H. Photovoltaic technology: The case for thin-film solar cells. *Science* **285**, 692–698 (1999).
10. Myong, S. Y., Kim, S. S. & Lim, K. S. Improvement of pin-type amorphous silicon solar cell performance by employing double silicon-carbide p-layer structure. *J. Appl. Phys.* **95**, 1525 (2004).
11. Soderstrom, T., Haug, F.-J., Niquille, X. & Ballif, C. TCOs for nip thin film silicon solar cells. *Prog. Photovolt. Res. Appl.* **17**, 165–176 (2009).
12. Kats, M. A., Blanchard, R., Genevet, P. & Capasso, F. Nanometre optical coatings based on strong interference effects in highly absorbing media. *Nature Mater.* **12**, 20–24 (2013).
13. Jin, H. *et al.* Efficient, Large Area ITO-and-PEDOT-free Organic Solar Cell Sub-modules. *Adv. Mater.* **24**, 2572–2577 (2012).
14. Guo, X. *et al.* Ultrathin and efficient flexible polymer photovoltaic cells based on stable indium-free multilayer transparent electrodes. *J. Mater. Chem.* **22**, 17176–17182 (2012).
15. Meyer, J., Zilberber, K., Riedl, T. & Kahn, A. Electronic structure of Vanadium pentoxide: An efficient hole injector for organic electronic materials. *J. Appl. Phys.* **110**, 033710 (2011).
16. Lassiter, B. E. *et al.* Organic photovoltaics incorporating electron conducting exciton blocking layers. *Appl. Phys. Lett.* **98**, 243307 (2011).
17. Logeewaran, V. J. *et al.* Ultrasoft Silver Thin Films Deposited with a Germanium Nucleation Layer. *Nano Lett.* **9**, 178–182 (2009).
18. He, Y., Chen, H.-Y., Hou, J. & Li, Y. Indene-C₆₀ Bisadduct: A New Acceptor for High-Performance Polymer Solar Cells. *J. Am. Chem. Soc.* **132**, 1377–1382 (2010).
19. O'Malley, K. M., Li, C.-Z., Yip, H.-L. & Jen, A. K.-Y. Enhanced Open-Circuit Voltage in High Performance Polymer/Fullerene Bulk-Heterojunction Solar Cells by Cathode Modification with a C₆₀ Surfactant. *Adv. Energy Mater.* **2**, 82–86 (2012).
20. Goerlitzer, M. *et al.* Ambipolar diffusion length and photoconductivity measurements on “midgap” hydrogenated microcrystalline silicon. *J. Appl. Phys.* **80**, 5111–5115 (1996).
21. Schiff, E. A. Low-mobility solar cells: a device physics primer with application to amorphous silicon. *Sol. Energy Mater. Sol. Cells* **78**, 567–595 (2003).
22. Deng, X. & Schiff, E. A. *Handbook of Photovoltaic Science and Engineering* (Chap. 12) [Luque, A. & Hegedus, S. (ed.)] [505–566] (John Wiley and Sons, Chichester, 2003).
23. Staebler, D. L. & Wronski, C. R. Reversible conductivity changes in discharge-produced amorphous Si. *Appl. Phys. Lett.* **31**, 292 (1977).
24. Branz, H. M. Hydrogen collision model: Quantitative description of metastability in amorphous silicon. *Phys. Rev. B* **59**, 5498–5512 (1999).
25. Deceglie, M. G., Ferry, V. E., Alivisatos, A. P. & Atwater, H. A. Design of Nanostructured Solar Cells Using Coupled Optical and Electrical Modeling. *Nano Lett.* **12**, 2894–2900 (2012).
26. Carlson, D. E. & Wronski, C. R. Amorphous silicon solar cell. *Appl. Phys. Lett.* **28**, 671 (1976).
27. Shah, A. V. *et al.* Thin-film silicon solar cell technology. *Prog. Photovolt. Res. Appl.* **12**, 113–142 (2004).
28. Benagli, S. *et al.* High-efficiency amorphous silicon devices on LPCVD-ZnO TCO prepared in industrial KAI-M R&D reactor. *24th European Photovoltaic Solar Energy Conference* (2009).

Acknowledgments

We acknowledge NSF ECCS for the support of this work. The study of the interfacial charge transport layers is supported by the Center for Solar and Thermal Energy Conversion, an Energy Frontier Research Center funded by the U.S. Department of Energy, Office of Science, Basic Energy Sciences under Award DE-SC0000957. The authors are grateful to Soluxra Inc. for providing the C₆₀ surfactant used in the experiment.

Author contributions

J.Y.L. exploited electrical hybrid device structures, fabricated the devices, and measured the electrical performances. K.-T.L. and S.S. carried out the numerical simulations, characterized the samples, and performed the optical measurements. L.J.G. guided the device design and the experiment. All authors contributed to discussion of the project and the manuscript.

Additional information

Supplementary information accompanies this paper at <http://www.nature.com/scientificreports>

Competing financial interests: The authors declare no competing financial interests.

How to cite this article: Lee, J.Y., Lee, K.-T., Seo, S. & Guo, L.J. Decorative power generating panels creating angle insensitive transmissive colors. *Sci. Rep.* **4**, 4192; DOI:10.1038/srep04192 (2014).



This work is licensed under a Creative Commons Attribution-NonCommercial-NoDerivs 3.0 Unported license. To view a copy of this license, visit <http://creativecommons.org/licenses/by-nc-nd/3.0>